









RESEARCH ARTICLE



Exosomes derived from neural progenitor cells preserve photoreceptors during retinal degeneration by inactivating microglia

Baishijiao Bian ^{a,b}, Congjian Zhao^{a,b}, Xiangyu He ^{a,b}, Yu Gong ^{a,b}, Chungue Ren^{a,b}, Lingling Ge ^{a,b}, Yuxiao Zeng ^{a,b}, Qiyu Li ^{a,b}, Min Chen^{a,b}, Chuanhuang Weng^{a,b}, Juncai He^{a,b}, Yajie Fang^{a,b}, Haiwei Xu ^{a,b,*} and Zheng Qin Yin ^{a,b,*}

^aSouthwest Hospital/Southwest Eye Hospital, Third Military Medical University (Army Medical University), Chongqing, P.R. China; ^bKey Lab of Visual Damage and Regeneration & Restoration of Chongqing, Chongqing, P.R. China

ABSTRACT

Retinal degeneration (RD) is one of the most common causes of visual impairment and blindness and is characterized by progressive degeneration of photoreceptors. Transplantation of neural stem/progenitor cells (NPCs) is a promising treatment for RD, although the mechanisms underlying the efficacy remain unclear. Accumulated evidence supports the notion that paracrine effects of transplanted stem cells is likely the major approach to rescuing early degeneration, rather than cell replacement. NPC-derived exosomes (NPC-exos), a type of extracellular vesicles (EVs) released from NPCs, are thought to carry functional molecules to recipient cells and play therapeutic roles. In present study, we found that grafted human NPCs (hNPCs) secreted EVs and exosomes in the subretinal space (SRS) of RCS rats, an RD model. And direct administration of mouse neural progenitor cell-derived exosomes (mNPC-exos) delayed photoreceptor degeneration, preserved visual function, prevented thinning of the outer nuclear layer (ONL), and decreased apoptosis of photoreceptors in RCS rats. Mechanistically, mNPC-exos were specifically internalized by retinal microglia and suppressed their activation *in vitro* and *in vivo*. RNA sequencing and miRNA profiling revealed a set of 17 miRNAs contained in mNPC-exos that markedly inhibited inflammatory signal pathways by targeting TNF- α , IL-1 β , and COX-2 in activated microglia. The exosomes derived from hNPC (hNPC-exos) contained similar miRNAs to mNPC-exos that inhibited microglial activation. We demonstrated that NPC-exos markedly suppressed microglial activation to protect photoreceptors from apoptosis, suggesting that NPC-exos and their contents may be the mechanism of stem cell therapy for treating RD.

ARTICLE HISTORY

Received 13 November 2019
Revised 12 February 2020
Accepted 1 March 2020

KEYWORDS



Extracellular vesicles; neural progenitor cells; exosomes; microRNAs; retinal degeneration; microglia

Introduction


Retinal degeneration (RD) including retinitis pigmentosa (RP) and age-related macular degeneration (AMD) is characterized by the photoreceptor loss and causes blindness in millions of people worldwide [1,2]. Although more than 250 genetic mutations and other changes in the retina contribute to RD development, the pathogenesis of RD is still unclear and there is no effective treatment strategy available.

Alternative strategies for RD treatment are under development, and stem cell therapy has been a particularly promising therapeutic candidate for treatment of RD. Many animal experiments and several phase I/II clinical trials have proven that stem cell transplantation can rescue or restore the vision of animals or patients with RD [3–5]. Wang et al. reported that transplantation of human neural

progenitor cells (hNPCs) derived from cortex restored the acuity and luminance thresholds of Royal College of Surgeons (RCS) rats for more than 8 months [4]. Similarly, we demonstrated in an earlier study that human retinal progenitor cells (hRPCs), one type of hNPCs isolated from human retina, significantly improved the visual acuity of five RP patients for 6 months after transplantation [6]. The transplanted stem cells are thought to differentiate and replace the degenerating cells [7,8], and the grafted NPCs are reported to differentiate to build the synaptic connections with the host retinal neurons [9,10]. But the proportion of daughter cells differentiated from NPCs that integrate into the neural circuits is extremely low and unlikely produce significant therapeutic effects. And recent studies have suggested that material exchange between the grafted stem cells and recipient's

CONTACT Haiwei Xu; Zheng Qin Yin  xuhaiwei@tmmu.edu.cn; qinzyin@aliyun.com  Southwest Hospital/Southwest Eye Hospital, Third Military Medical University (Army Medical University), Chongqing 400038, P.R. China

*These authors contributed equally to this work.

 The supplemental data for this article can be accessed [here](#).

© 2020 The Author(s). Published by Informa UK Limited, trading as Taylor & Francis Group on behalf of The International Society for Extracellular Vesicles. This is an Open Access article distributed under the terms of the Creative Commons Attribution-NonCommercial License (<http://creativecommons.org/licenses/by-nc/4.0/>), which permits unrestricted non-commercial use, distribution, and reproduction in any medium, provided the original work is properly cited.

cells is likely the major efficient approach to rescue degeneration [11–13]. Our recent study found that grafted mouse NPCs (mNPCs) delayed the degeneration of photoreceptors and promoted a protective retinal microenvironment during RD by suppressing the activation of microglial cells [14], but the mechanisms through which the NPCs suppress the microglial activation in RD require further clarification.

Exosomes, carrying the classic markers CD63, CD81 and CD9 can mediate intercellular communication between grafted stem cells and recipient's cells [15,16]. Webb et al. reported that the exosomes released from grafted NPCs (NPC-exos) exerted neuroprotective effects in CNS disorders, including Alzheimer's disease (AD) and stroke [17–19]. Exosomes induce tissue regeneration and reduce inflammation by delivering their functional cargo, such as microRNAs (miRNAs), mRNAs, lipids, and various proteins [20–22]. Many studies have demonstrated that miRNA delivery by exosomes regulates grafted cells in the recipient [23,24]. It is possible, therefore, that the exosome cargoes are somehow mediating the observed effects of grafted NPCs during RD therapy.

In this study, we found that the neuroprotective role of grafted NPCs was associated with the secretion of exosomes in the subretinal space (SRS) of RCS rats, and subretinal injection of mNPC-exos delayed the progression of RD in this RD model. It confirmed that exosomes derived from mNPCs (mNPC-exos) could be specifically internalized by microglia, and protected photoreceptors from apoptosis both *in vivo* and *in vitro*. mRNA sequencing (mRNA-seq) of microglia, miRNA profiling of exosomes, and ingenuity pathway analysis (IPA) revealed a set of 17 miRNAs enriched in NPC-exos that inhibited inflammatory signal pathways in microglia by targeting TNF- α , IL-1 β and COX-2. Collectively, our results suggest that NPC-exos may be mediating the observed effects of NPC grafts in an RD model, and that these exosomes may be anovel therapeutic agent.

Materials and methods

Animals

RCS rats regardless of sex and female C57BL/6 mice were provided by the Experimental Animal Center of Third Military Medical University (Army Medical University) and were raised in the specific pathogen-free room in the Animal Care Center of Southwest Hospital. All animal work in this study was approved by the Ethical Committee of Southwest Hospital, Third Military Medical University (Army Medical University) and were in accordance with the Helsinki Declaration. Three individuals were used for each experiment at least.

Cell culture and co-culture system

Primary mNPCs were isolated from the subventricular zone (SVZ) of C57BL/6 mice. The culture conditions for mNPC, and lentiviral infections were according to previous description [25].

BV2 cell, a mouse microglia cell line, was provided by Dr. Guo from Neurological Surgery of Southwest Hospital. 661 W cell, a mouse photoreceptor-like cell line, was gifted by Dr. Al Ubaidi (University of Oklahoma, Norman, USA) [26]. Both BV2 microglia and 661 W cells were cultured with high-glucose Dulbecco's modified Eagle's medium (high-glucose DMEM) (Cat. No. SH30022.01, HyClone) with 10% foetal bovine serum (FBS) (Cat. No. VS500 T, Ausbian) and 1% penicillin-streptomycin (PS) (Cat. No. 10010049, Thermo Fisher Scientific) [14,27]. BV2 microglia for RT-qPCR were seeded in 6-well plate at a density of 2×10^5 cells/well. To prepare the co-culture system, the 661 W cells were seeded at a density of 2×10^5 cells/well in 6-well plates and cultured for 24 h and co-cultured with conditioned BV2. BV2 cells were seeded in the transwell chambers (Cat. No. MCRP24H48, Millipore) at a density of 2×10^4 cells/chamber or 1×10^5 cells/plate for 6 h before treatment with lipopolysaccharides (LPS, 1 μ g/mL) (Cat. No. L4516, Sigma) for 24 h. For further incubation with mNPC-exos, BV2 chambers were washed with warmed PBS (Cat. No. SH30256.01, Hyclone), moved into 661 W wells, added fresh mNPC-exos in the upper chamber and co-cultured till 48 h for further assay.

Human NPC were isolated from human embryonic retina which was provided by the embryonic tissue bank of the Department of Obstetrics in Southwest Hospital [5]. All experiments involving in human tissues and cells were approved by the ethics committee of Southwest Hospital. The hNPCs were harvested from the foetal retinas as previously described [28] and cultured in the UltraCULTURE medium (Cat. No. 12-725 F, Lonza) with 20 ng/mL human FGF (Cat. No. AF-100-18B-100, Peprotech), 10 ng/mL human EGF (Cat. No. AF-100-15-100, Peprotech), 1% Glutamax (Cat. No. 35050061, Gibco) and 1% PS.

The immortalized human microglia-SV40 cell line was acquired from Applied Biological Materials, Inc. (ABM, T0251) and cultured, as previously described, in the high-glucose DMEM culture medium [13].

The five cells used in this study were tested for endotoxin contamination and mycoplasma contamination before further experiments and they were negative.

Vector production, lentivirus package, titration, mNPC-infection and exosome labelling

Plasmids, RRE, ADV, REV, VSVG and Lenti-CMV-CD63-RFP (a kind gift from Dr. Stefano Pluchino, University of

Cambridge) were used for lentivirus package in HEK293T cells, as described [29,30]. The viral supernatant was concentrated and detected the titration with HEK293T cells. mNPC single cells were infected with the lentivirus at P2 with 10 multiplicity of infection (MOI). The high efficiency of the labelling was confirmed by confocal microscope (Figure S3a) and the non-significant influence of the lentivirus infection on the proliferation of mNPCs was verified by cell proliferation experiment (Figure S3b).

The exosomes were labelled with PKH26 Red Fluorescent Cell Linker Kit (Cat. No. MINI26, Sigma). In brief, exosome pellet was resuspended with 1 mL diluent C and mixed with solution A (4 μ L PKH26 dye in 1 mL diluent C). 2 mL 1% BSA was added into the mixture after 5 min staining. The mixture with exosomes were layered upon 1.5 mL 0.9 M sucrose solution and 7 mL PBS. Exosome pellet was resuspended with 100 μ L PBS after 200,000 \times g for 2 h. Further, to remove the extra dye, exosome spin columns (Cat. No. MW3000, Thermo Fisher Scientific) were used as the manufacturer's protocol described.

Exosomes isolation

mNPCs were dissociated into single cell and plate in flask for 24 h at a density of 1×10^7 cells per 10 mL culture medium per T75 culture flask. Culture supernatant was harvested and centrifuged at 1,500 rpm for 15 min and at 2,500 rpm for 15 min at 4°C to remove cellular debris. To further harvest the EV, the supernatant was centrifuged at 100,000 \times g for 70 min at 4°C (Beckman OPTIMA XPN-100, SW 28Ti Swinging-Bucket Rotor). To purify the exosomes, EV pellet was resuspended with 0.32 M sucrose solution and layered on the top of a continuous sucrose density gradient (2.0–0.32 M sucrose, 5 mM HEPES, pH = 7.4) and centrifuged at 100,000 \times g for 16 h at 4°C using a Beckman OPTIMA XPN-100, SW 40Ti Swinging-Bucket Rotor. Fractions (1 mL per fraction) were gathered from the top which has low density to the bottom of the tube of the sucrose gradient. Fractions ranging from 1.13 to 1.20 g/mL from the gradient were collected, diluted in 5 mM HEPES, centrifuged at 100,000 \times g for 70 min (Beckman OPTIMA XPN-100, SW 28Ti Swinging-Bucket Rotor). Pellet was resuspended with normal saline (for transplantation *in vivo*) or PBS (for experiments *in vitro*). Every 10 mL culture medium was concentrated to 10 μ L.

Transmission electron microscopy (TEM)

Exosomes purified from 10 mL mNPC or hNPC culture medium were suspended in 100 μ L PBS and pipetted (50 μ L) onto the formvar-coated copper

grids and allowed to settle for 20 min at ambient temperature. Samples were fixed in a solution of 2% paraformaldehyde, 2% glutaraldehyde, and 0.05 M phosphate solution for 2 minutes. Grids were washed three times with distilled water before application of 1% phosphotungstic acid (PTA) and were counterstained for one minute. Wicking with filter paper to remove excess liquid, and the grids were dried overnight and were analysed by a transmission electron microscopy (JEM-1400PLUS, Japan).

Nanoparticle tracking analysis (NTA)

1 μ L fresh concentrated exosome solution was diluted in 1 mL PBS, gently pipetted for 10 s and injected into a Nanosight NTA NS300 instrument (Malvern Instruments Ltd.) using a sterile injection syringe. And the dynamic images were recorded and analysed to obtain the concentration and distribution of the particles.

Western blot (WB)

1 μ L fresh concentrated exosome solution was diluted in 50 μ L PBS, and protein concentration was measured by BCA assay. Equal amounts of exosomes were loaded and separated on a 12% SDS-PAGE gel. And the electrophoresis was conducted at 80 V for stacking and 100 V for separation. After being transferred to a PVDF membrane, the samples were blocked with 5% skimmed milk in TBST buffer (20 mM Tris base, 150 mM NaCl and 0.1% Tween 20) for 30 min and incubated with primary antibodies overnight at 4°C. Membranes were further incubated with HRP-conjugated secondary antibodies for 1 h at ambient temperature. Antibodies against CD63, CD9, CD81, HSP70 and goat anti-rabbit HRP secondary antibody (SBI System Biosciences (EXOAB-CD63A-1,1:000; EXOAB-CD9A-1, 1:1000; EXOAB-CD81A-1,1:1000, EXOAB-Hsp70A-1,1:1000, goat anti-rabbit HRP secondary antibody, 1:2000) were applied in the blotting.

Subretinal transplantation

Subretinal transplantations were performed in RCS rats (postnatal 21 days) with CD63-RPF labelled mNPC-exos or EGFP-labelled hNPCs. One eye of RCS rats was injected with 1 μ L concentrated mNPC-exos resuspended solution that contained $1.09e + 011 \pm 4.99e + 009$ exosomes or 2 μ L concentrated hNPCs contained 2×10^5 cells. And the other eye was injected with normal saline (vehicle). The retinas which did not receive any injections were untreated group. All RCS

rats, including that in untreated group, received oral cyclosporine A (210 mg/L) (Sandoz, UK) dissolved in drinking water from 24 h before transplantation to day 14 post-injection.

Immunofluorescence staining (IF)

For mNPC spheres preparation, mNPC (Passage 8) spheres were collected via centrifuging, fixed in 4% PFA for 30 min at 4°C. RCS rats were euthanized at 2, 4, 7, 14 days after transplantation by carbon dioxide inhalation, and eyes were removed for tissue preparation as described previously [13]. These eyes cups and the mNPC spheres were fixed in 4% PFA for 4 h at 4°C and dehydrated in 30% glucose solution overnight. Frozen sections were cut from tissue embedded in the optimum cutting temperature (OCT) compound and preserved and attached to glass slides. For cultured cells, BV2 and 661 W slides were fixed in 4% PFA for 15 min at ambient temperature and washed with PBS.

IF of frozen sections and fixed cell slides were performed as described previously [13]. In brief, sections were air dried, washed in PBS. Cell slides and sections were blocked with 0.3% Triton X-100 (Cat. No. P0096, Beyotime Biotechnology,) and 3% albumin from bovine serum (BSA) at 37°C for 30 min and then incubated with primary antibodies at 4°C overnight. And the slides were incubated with secondary antibodies at 37°C for 40 min. And the slides were staining with 4',6-diamidino-2-phenylindole (DAPI) (Cat. No. C1005, Beyotime Biotechnology), and scanned and photographed via a confocal microscopy (Leica SP8). The antibodies and dilutions have been used in our study: APC anti-human CD63 (Cat. No. 353008, Biolegend, 1:100), mouse anti-RPE65 (Cat. No. ab78036, Abcam, 1:500), rabbit anti-GS (Cat. No. ab73593, Abcam, 1:500), rabbit anti-Iba1 (Cat. No. 019-19741, Wako, 1:500), mouse anti-Nestin (Cat. No. ab6142, Abcam, 1:200) rabbit anti-PAX6 (Cat. No. ab5790, Abcam, 1:500), rabbit anti-Sox2 (Cat. No. ab97959, Abcam, 1:500), mouse anti-TUJ1 (Cat. No. AT809-1, Beyotime Biotechnology, 1:500), rabbit anti-Recoverin (Cat. No. ab101584, Abcam, 1:500), rabbit anti-GFAP (Cat. No. ab48050, Abcam, 1:500), goat anti-mouse IgG Alexa-Fluor-647 (Cat. No. A21236, Life technologies, 1:1000), goat anti-rabbit IgG Alexa-Fluor-488 (Cat. No. A11001, Life technologies, 1:1000) and goat anti-mouse IgG Alexa-Fluor-488 (Cat. No. R37120, Life technologies, 1:1000).

Optokinetic response (OKR) test

RCS rats at days 2, 4, 7, 14, 21 and 28 post-operation, postnatal 23, 25, 28, 35 and 42 days, were dark-adapted for at least 16 h before OKR test, as previously described

[13,31]. Briefly, a platform was set as shown (Figure S2), the RCS rat was placed on the platform and stimulated with a rotated grating using a staircase paradigm program written with MATLAB display spatial frequencies of 0.05, 0.075, 0.1, 0.2, 0.3, 0.4, 0.5 and 0.6 cycles/degree in 100% contrast to measure the visual acuity in both eyes. The head tracing of clockwise or counter-clockwise rotations were recorded by the video camera. The minimum mean luminance of the monitor screens was 0.02 cd/m² and the maximum was 50 cd/m². And the highest spatial frequency with a single-side (clockwise or counter-clockwise) rotation was recorded as the visual acuity of the responsive eye.

Scotopic electroretinogram (ERG) Recording

The scotopic ERG was carried out at days 2, 4, 7, 14, 21 and 28 post-operation, as described previously [13]. In brief, RCS rats were dark-adapted for at least 16 hours and anaesthetized before ERG test. The animals were prepared for recording under dim red-light (wavelength > 620 nm). The gold cornea electrodes were placed attaching to the corneas as recording electrodes. And the reference and ground electrodes were placed subcutaneously in the cheek area and tail, respectively. Light stimuli were rendered at intensities of -2.5, -0.5, -0.02, 0.5 and 1 log (cd*m/s²). A RETI-Port device (Roland Consult) was used to record the response of each flash. The amplitude of the a-wave was measured as the maximum negative trough below the baseline. The b-wave was calculated from the a-wave trough to the maximum subsequent positive peak.

TUNEL staining

The slides were incubated with DAPI (Cat. No. C1005, Beyotime Biotechnology) and apoptotic cells of retina and 661 W were detected using *in situ* cell death detection kit (Roche, 11684795910). All processes were conducted according to the manufacturer's protocol. And slides were then observed under a confocal microscope (Leica SP8).

Analysis of outer nuclear layer (ONL)

The sections of entire retinas were stained with DAPI and TUNEL, scanned by the confocal microscope and measured maximum intensity z-projection (layer = 10) with ImageJ software (NIH). 400× field views of corresponding group (mNPC-exo-injected area, mNPC-exo-non-injected area, vehicle-injected area, vehicle-non-injected area) were analysed to obtain the absolute and percentage numbers of ONL nucleus with ImageJ software. Three sections from three eyes were included in each group. To evaluate the thickness of ONL in each group, the z-projected entire retina section images were analysed. Each

optic nerve head (ONH) was defined as the original location (recorded as 0). And three 400× field views (from three retinas) of ONL at different positions (inject area: 2, 4, 6, 8, 10 ×400 μm; non-injected area: -2, -4, -6, -8, -10 ×400 μm; as Figure 1(b) shown) were analysed to obtain the number of cell layers in ONL as previously described [4,32].

Analysis of microglia

Three 400× field views from three retinas per group were captured at the injected area using a confocal microscope at 0.5 μm intervals (Leica SP8) and measured maximum intensity z-projection (layer = 10) with ImageJ software. Iba1⁺ microglial cells were calculated with ImageJ and obtained the density of microglia in ONL and SRS per mm³. And a grid system was used to analyse the morphology of microglial cells in the SRS [33,34]. 6 microglial cells in SRS from each retina were analysed to determine the number of grid-crossing points per cell. And 3 retinas were contained in each group.

Flow cytometry (FCM)

For apoptosis assay, isolated 661 W cells were stained with Annexin V (Cat. No. 550474, BD Biosciences) and PI (Cat. No. 556547, BD Biosciences) as the manufacturer's instructions described.

For identification, primary hNPCs were isolated at Passage 4 as single cells at a concentration of 1 × 10⁶/100 μL (a test) were incubated with FITC-conjugated primary antibodies including PAX6 (Cat. No. 561664, BD Biosciences), Nestin (Cat. No. 4335384, Invitrogen), Sox2 (Cat. No. 5619593, BD Biosciences), and κ Isotype Control antibody (20 μL/test) (Cat. No. 555578, BD Biosciences) at 4°C for 1 h, as previously described [28]. After being washed with Wash Buffer (Biolegend), hNPCs were harvest via centrifugation. The hNPCs were resuspended with 300 μL PBS and transferred to a flow cytometry tube for FCM analysis. All FCM assays were performed via BD FACS Calibur and BD FACS Aria II flow cytometer, and FlowJo software was used to analyse the data.

Lactate dehydrogenase (LDH) release assay

To assess photoreceptor death, LDH release in supernatant of 661 W cells was detected (Cat. No. C0016, Beyotime Biotechnology). The supernatant of 661 W cells in six-well plate, co-cultured with conditioned BV2 for 48 h, was collected for detection, as the manufacturer's protocol described.

RNA isolation and reverse-transcription quantitative polymerase chain reaction (RT-qPCR) analysis

Total RNAs of BV2 cells were extracted and using RNAiso Plus (Cat. No. D9108A, Takara) as the manufacturer's instructions. And small RNAs of exosomes derived from mNPCs or hNPCs were extracted and isolated with a miRNeasy Mini Kit (Cat. No. 217004, Qiagen). PrimeScriptTM RT reagent kit (Cat. No. #RR037A, Takara) was used to reverse the RNA samples as the manufacturer's instructions. The expression of each gene was measured with RT-qPCR as previously described [13]. And the results were normalized to GAPDH levels. All primers were listed in Table S3. The mean and standard deviation were calculated from nine independent experiments.

miRNA and mRNA sequencing and analysis

For exosome miRNA sequencing, RNA was isolated by Trizol extraction from exosomes of mNPCs and hNPCs. And Agilent Bioanalyzer small RNA assay kit (Novogene) was used to quantify the samples. And libraries were prepared according to manufacturer's protocol (Illumina small RNA preparation kit), as previously described [35]. Three experimental replicates per group were performed. For the transcriptome study, all samples were transported to the Novogene Experimental Department in dry ice box.

The poly-T oligo-attached magnetic beads were used to purify mRNAs from total RNAs. Divalent cations were carried out the fragmentation in NEBNext First Strand Synthesis Reaction Buffer (5X) under elevated temperature. And the cDNA libraries were produced on a cBot Cluster Generation System using TruSeq PE Cluster Kit (Illumina) according to the manufacturer's instructions. Then the library preparations were sequenced on an Illumina HiSeq platform and 125 bp/150 bp by paired-end reads were generated. The Pearson correlation coefficients were based on all gene expression levels. A heatmap analysis of gene expression levels was created based on the averaged fragments per kilobase of exon per million fragments mapped (FPKM) values of genes in microglia with or without mNPC-exos stimulated by LPS. The KEGG database was used to perform pathway analysis of differentially expressed genes.

Enzyme-linked immunosorbent assay (ELISA)

The levels of TNF-α (LEGEND MAXTM Mouse TNF-α ELISA Kit, Biolegend), IL-1β (Mouse IL-1β Elisa kit,

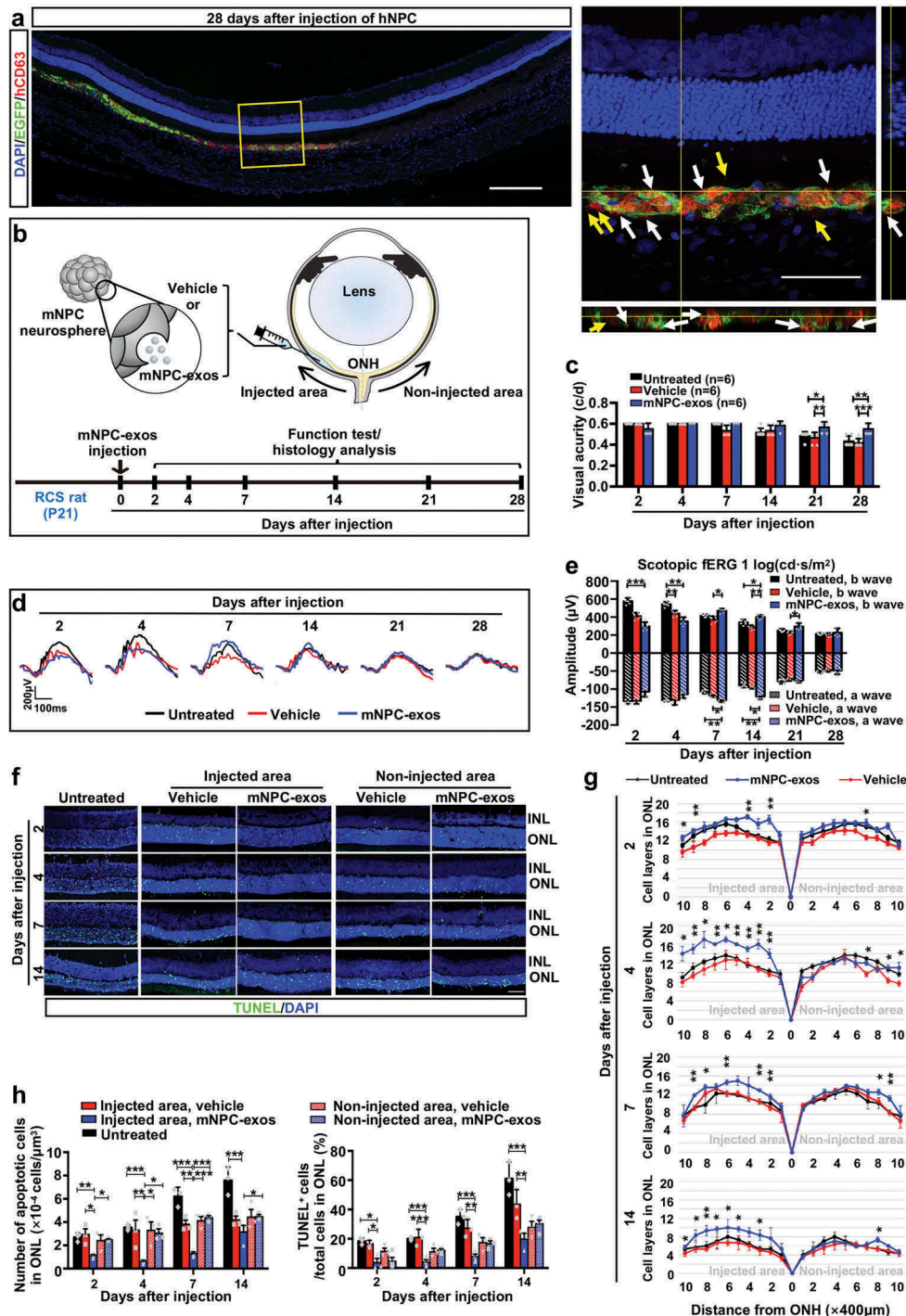


Figure 1. Implantation of NPC-exos preserve visual function and protect photoreceptors from apoptosis in RCS rats.

(a) The immunofluorescence staining of human CD63, the marker of exosomes derived from hNPC-exos, in RCS retinal section derived from the eyes of RCS rats subretinally injected with EGFP-labelled hNPC for 28 days. Left panel showing the EGFP⁺ hNPC (green) and hCD63 positive hNPC derived EVs and exosomes (red) in the grafted area (scale bar, 200 μ m). Right panel: enlarged image and orthogonal view of confocal image showing hNPC derived EVs and exosomes (red) are inside of, at the surface of (white arrowed), and out of (yellow arrowed) hNPCs (scale bar, 50 μ m). See also Movie S1.(b) Diagram illustrating the subretinal transplantation (upper panel). Scheme of time points for mNPC-exos or vehicle injection, function test and histology analysis (lower panel).(c) Visual acuity measured through the optokinetic response test in mNPC-exos, vehicle and untreated groups at days 2, 4, 7, 14, 21 and 28 post-injection ($n = 6$ eyes per group).(d) Representative scotopic fERG waveforms elicited at 1 log(cd*s/m²) light intensity measured mNPC-exos, vehicle and untreated groups at 2, 4, 7, 14, 21 and 28 days post-injection ($n = 6$ eyes per group).(e) Statistical analysis of scotopic fERG a- and b-wave amplitudes elicited at 1 log(cd*s/m²) light intensity in three groups at each time point ($n = 6$ eyes per group). Since a-waves of fERGs are negative, then a-wave amplitudes are presented on the lower, negative axis.(f) Apoptosis detection by TUNEL and DAPI staining in RCS retinas (inner nuclear layer, INL, and outer nuclear layer, ONL) of mNPC-exos, vehicle and untreated groups at days 2, 4, 7 and 14 post-injection. Scale bar, 50 μ m.(g) Numbers of cell layers in ONL were compared in mNPC-exos, vehicle and untreated groups at different locations, distance from optic nerve head (ONH), at each time point ($n = 3$ per group). Untreated vs vehicle: no significant. mNPC-exo vs Vehicle: * $P < 0.05$, ** $P < 0.01$ (h) Numbers of apoptosis cells (left panel) and the percentage of TUNEL positive cells (right panel) in ONL were statistical analysed in mNPC-exos, vehicle and untreated groups (including injected area and non-injected area) at each time point ($n = 3$ per group). Untreated vs vehicle: no significant. mNPC-exo vs Vehicle: * $P < 0.05$, ** $P < 0.01$, *** $P < 0.001$.Data are shown as mean \pm SD.

Dakewe Biotech Co. 1210122) and COX2 (Prostaglandin E2 Express ELISA Kit, Cayman #500141) in the supernatant of BV2 cell culture adding LPS with or without mNPC-exos were quantified using ELISA kits. The kits were used as described previously [14].

Statistical analysis

All data were presented as the mean \pm SD (standard deviation) from at least three biological samples. Statistical Product and Service Solutions software V25.0 (SPSS V25.0) was applied for statistical analysis. Statistical differences were measured with Student's t-test for comparison between two groups or analysis of variance (ANOVA) for comparison of multiple groups by Turkey's t-test or Dunnett's T3 multiple comparison tests. P values < 0.05 were considered to be significant.

Results

Implantation of mNPC-exos reduce apoptosis of photoreceptors to preserve visual function in RD model

To investigate whether grafted NPC secrete exosomes, human CD63, a feature molecule of human EVs and exosomes, was stained with IF on retina sections derived from the eyes of RCS rats subretinally injected with EGFP-labelled hNPC for 28 days. We found that human CD63⁺ EVs and exosomes localized at the outside, surface and inside the grafted hNPCs (Figure 1(a) and Movie S1), indicating that grafted hNPCs secreted EVs and exosomes. We then investigated whether NPC-exos exerted therapeutic effects during RD in RCS rats and explored the relative mechanism, so we performed *in vivo* experiments with mNPC. To gain exosomes, mNPCs were isolated from the SVZ of adult mice, which were identified as positive expression for expression of Nestin (Figure S1a), PAX6, and SOX2 (Figure S1b), and could be induced to differentiate into neurons (TUJ1⁺) and glial cells (GFAP⁺) after 7 days (Figure S1c). Differential centrifugation and sucrose gradient density centrifugation were used to purify mNPC-exos, which were identified as positively expressing of the specific markers HSP70, CD63, CD9 and CD81 by WB (Figure S1e). TEM showed that the mNPC-exos presented typical cup-shaped membrane vesicles with diameters from 50 to 180 nm (Figure S1f). NTA revealed that the purified mNPC-exos were relatively homogeneous particles (Figure S1g, left

panel) with a peak of 99 nm diameter and an average size of 97.9 ± 0.7 nm (Figure S1g, right panel).

We then injected 1 μ L of concentrated mNPC-exos solution (containing $1.09e + 009 \pm 4.99e + 007$ exosomes) per eye into SRS of RCS rats and performed OKR (Figure S2) and scotopic ERG test. OKR showed that mNPC-exo treatment significantly rescued the visual acuity of RCS rats (detectable maximum 0.6) at days 21 and 28 post-injection, compared with the vehicle or untreated control that both had similar visual acuity (Figure 1(c)). The scotopic ERG at 1 log (cd*s/m²) showed that compared to the vehicle group, the injection of mNPC-exos significantly preserved the amplitudes of both a-wave and b-waves at day 7 after injection and that this effect was maintained to day 21 post-injection (Figure 1(d, e)). It is notable that amplitudes of a-wave and b-wave at days 2 and 4 in mNPC-exos and vehicle groups were smaller than in the untreated group, implying that the injection might induce a damage.

It has been reported that *Mertk* mutation-derived dysfunction of RPE results in apoptosis of photoreceptors and reductions thickness and cell layers of ONL in RCS rats [36]. So, we investigated the effects of mNPC-exos on apoptosis of photoreceptors and the degeneration of ONL. We found that the thickness and the layers of ONL around the injected area were significantly preserved in the mNPC-exo group from day 4 to 14 post-injection, compared with that in the vehicle and untreated groups (Figure 1(f, g)), while a similar thickness and layer of ONL in the non-injected area in these two groups were observed. TUNEL staining revealed that mNPC-exo treatment significantly reduced the number of TUNEL⁺ cells around the injected area, compared with the untreated, vehicle group and the non-injected area of mNPC-exos treated eyes at days 2, 4, 7 and 14 post-injection, respectively (Figure 1(h), left panel). Consistently, the percentage of TUNEL⁺ cells in ONL rats were significantly reduced in mNPC-exos injected areas, compared with the vehicle and untreated groups from day 2 to 14 post-injection (Figure 1(h), right panel). These results demonstrate that grafted mNPC-exos preserve the photoreceptors from apoptosis to protect the visual function in an RD model.

Grafted mNPC-exos are specifically internalized by retinal microglia and suppress their activation in RD model

In order to explore how mNPC-exos protected photoreceptors from degeneration and apoptosis, we traced the grafted mNPC-exos labelled with CD63-RFP in the

retina of RCS rats. In the retina sections of mNPC-exo-treated RCS rats, the RFP-labelled mNPC-exos were observed in the SRS from day 2 to 14 post-injection, compared to the vehicle group (Figure 2(a)). In the mNPC-exo-treated group, the distribution of labelled mNPC-exos varied with the time course in the SRS. The mNPC-exos showed a diffuse distribution at day 2 (Figure 2(ai')), but at day 4 the mNPC-exos were enriched around the DAPI⁺ nucleus (Figure 2(aii')). The enriched mNPC-exos decreased gradually at days 7 and 14 (Figure 2(aiii', iv')). These results suggested that the RFP labelled exosomes are internalized by some cells with nuclei in SRS but not the photoreceptors in ONL.

To specify the cell type that internalized mNPC-exos in RCS retina, we stained the classical phagocytosis cells, including the Müller cells, RPE cells and microglia [37], in the retina at day 4 post-injection. IF showed that RFP-labelled exosomes did not co-localize with the GFAP⁺ Müller cells (Figure 2(b)) or RPE cells but did co-localize with Iba1⁺ microglial cells (Figure 2(c)).

Moreover, we observed that microglial cells gradually migrated from the inner retina to the ONL and SRS from day 2 to 14 post-injection in untreated and vehicle groups (Figure 3(a, left and middle panel, b)). Compared to the untreated and vehicle group, the mNPC-exos treated group showed a similar number of migrated microglia at day 2 in ONL and SRS. However, compared to the untreated and vehicle group, the number of migrated microglia in ONL and SRS was markedly reduced at days 7 and 14, although it was significantly increased at day 4. This might be due to an immune response induced by the xenograft (Figure 3(a, middle panel, b)).

We also observed that mNPC-exos were present in the SRS at day 2. At day 4 post-injection, a large number of migrated microglial cells were observed as round-shaped, a morphology of activation and internalizing mNPC-exos (Figure 3(a), middle panel and upper-enlarged panel). The internalized exosomes were markedly reduced in the microglia at day 7, but the morphology of microglia became ramified (Figure 3(a), middle panel and lower-enlarged panel). The morphology of microglia in both vehicle and mNPC-exo groups at days 4, 7 and 14 post-injection was further quantified with a grid system. The grid-crossed points per microglia cell in mNPC-exo group were significantly more than that in the untreated and vehicle group at days 7 and 14 post-injection (Figure 3(c, d)). Taken together, these results suggest that the grafted mNPC-exos can be specifically internalized by microglia and thereby suppress activation of the microglia.

Functional inhibition of microglial activation by mNPC-exos protects photoreceptors from apoptosis *in vitro*

We then confirmed whether mNPC-exos could inhibit microglia activation and preserve photoreceptors in a co-culture system composed of LPS-activated BV2, a mouse microglia cell line, and 661 W, a mouse photoreceptor cell line (Figure 4(a)). LPS treatment turned BV2 cells from spindle-shaped with long processes into round-shaped (Figure 4(bii)), implying that the BV2 cells were activated. Meanwhile, the activated BV2 cells extend with process after internalizing the grafted mNPC-exos (Figure 4(biii-v)), indicating that the activated BV2 cells were suppressed by mNPC-exos. As it is well known that activation of microglia results in the release of pro-inflammatory cytokines [38,39], we further evaluated the expression of pro-inflammatory cytokines TNF- α , IL-1 β and IL-6, as well as the anti-inflammatory cytokines Arg1, Ym1 and Fizz1 under LPS and mNPC-exo treatment at mRNA level with qRT-PCR. LPS stimulation markedly increased the levels of TNF- α , IL-1 β and IL-6 mRNA and decreased levels of Ym1 and Fizz1 mRNA compared to the control group, while mNPC-exos treatment significantly reversed the effect of LPS stimulation (Figure 4(c)). These results suggest that mNPC-exo suppress the LPS-induced activation of microglia *in vitro*.

Next, we analysed the influence of activated BV2 cells on apoptosis of 661 W cells in the co-culture system using TUNEL staining. We found that TUNEL-positive 661 W cells were markedly increased in the LPS treated group compared to the untreated group (Figure 4(d, e)). The LPS-stimulated group treated with mNPC-exos for 48 hours had a markedly reduced number of apoptotic 661 W cells. In line with this, FCM analysis showed that, compared with untreated BV2 group, the live 661 W cells were significantly decreased and the apoptotic cells were markedly increased in LPS-stimulated BV2 group. Compared with LPS-stimulated BV2 group, the live 661 W cells were significantly increased and the apoptotic cells were markedly reduced in mNPC-exos-treated BV2 group (Figure 4(f), Figure S4). In addition, an LDH release assay was used to assess neuronal cell death [40]. 661 W cells co-cultured with LPS-treated BV2 released more LDH in the medium than the co-culture with LPS-untreated BV2. mNPC-exos treatment markedly reduced the LDH release in 661 W cells co-cultured with LPS-stimulated BV2, compared to the mNPC-exo-untreated group (Figure 4(g)). These results suggest that mNPC-exos can reduce the apoptosis of photoreceptors induced by LPS-activated microglia *in vitro*.

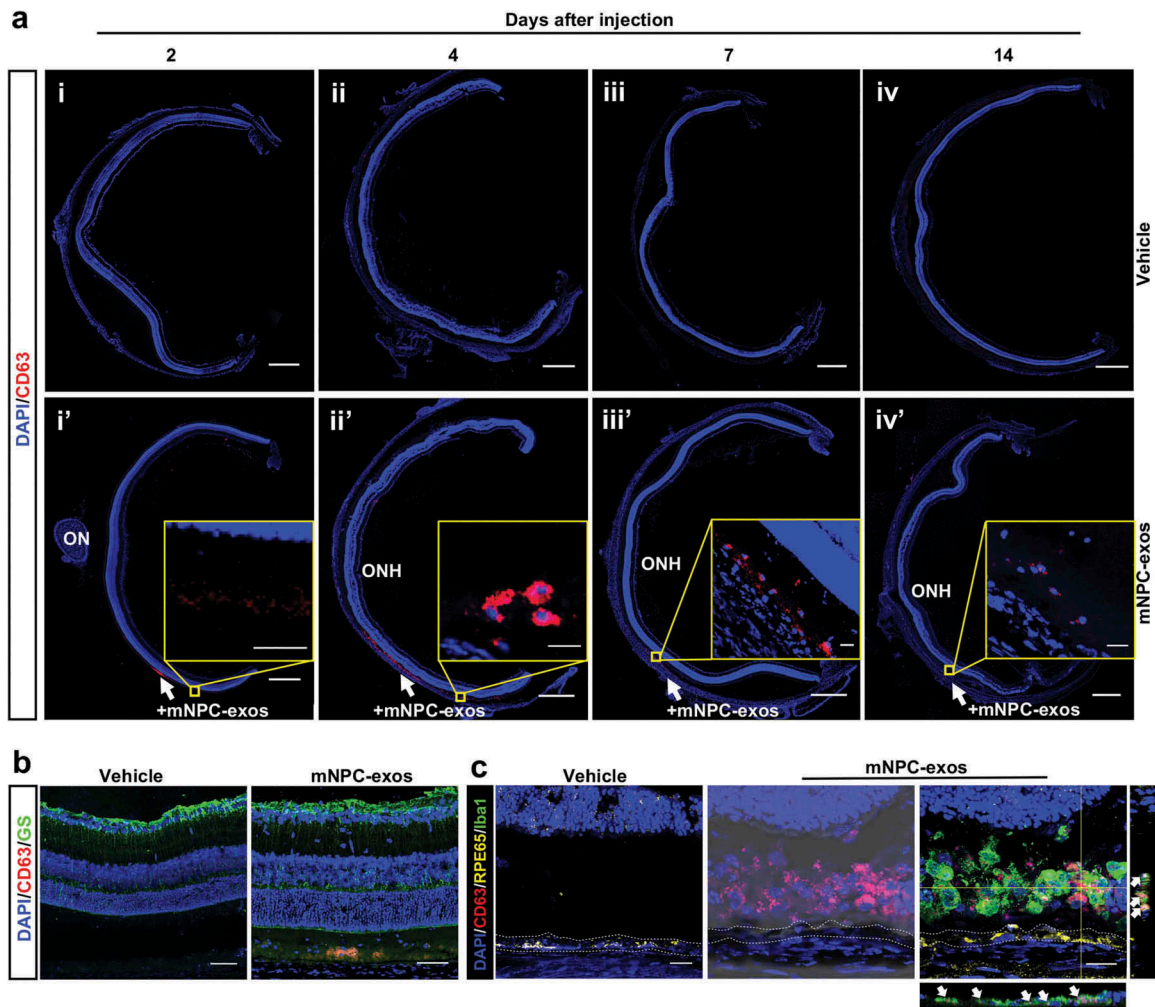


Figure 2. Grafted mNPC-exos were specifically internalized by retinal microglia.

(a) Confocal images showing RCS retina injected with vehicle (i,ii,iii,iv) and CD63-RFP (red) labelled mNPC-exos (i',ii',iii',iv') in subretinal space (SRS) at days 2 (a,b), 4 (c,d), 7 (e,f) and 14 (g,h) (scale bar, 500 μ m). White arrows: the direction and inject area. In mNPC-exos treated group, enlarged images showing the distribution of grafted exosomes at each time points (scale bar, 20 μ m). (b) The immunofluorescence staining of GS (green), the marker of Müller cell, in RCS retinal section 4 days after transplantation with vehicle (left) or CD63-RFP labelled mNPC-exos (right panel, red). Scale bar, 50 μ m. (c) The co-staining of RPE65 (yellow) and Iba1 (green), the marker of RPE cells and microglia respectively, in RCS retinal section of 4 days after injection with vehicle (left) or CD63-RFP labelled mNPC-exos (middle and right, red). The overlap of bright field image and immunofluorescence image (middle) shows mNPC-exos (red) locate outside of RPE cells. The orthogonal view shows mNPC-exos (red) co-locate with microglia (green). Scale bar, 50 μ m.

mNPC-exos inhibit inflammation signal pathways in activated microglia

To further define the underlying mechanism of inactivation of microglia, differentially expressed genes (DEGs) in BV2 cells treated with LPS and BV2 cells treated with LPS + mNPC-exos were identified by mRNA-seq. mNPC-exos treatment resulted in 2,034 DEGs, of which 1,182 were upregulated and 852 were downregulated (Figure 5(a)). The inflammation-related genes CCL3 ($2^{0.77}$ fold) and COX-2 ($2^{0.65}$ fold) were among the significantly down-regulated genes (Figure 5(b)). KEGG pathway analysis of the down-regulated genes revealed that mNPC-exos target

genes were involved in several inflammation-related pathways, including MAPK, IL-17, NK-kappa B and TNF pathways (Figure 5(c)). In addition, IPA of these DEGs showed that mNPC-exo target genes were involved in 580 ingenuity canonical pathways (Table S1). Among them, clathrin-mediated endocytosis signalling was significantly regulated by mNPC-exos (Figure S5a), which is consistent with previous studies about cellular uptake of exosomes [41,42]. Focusing on inflammation-related pathways, it was predicted that Fc γ receptor-mediated phagocytosis in macrophages and monocytes and interferon signalling were activated (Figure S5b), while more pathways were inhibited, including neuroinflammation signalling

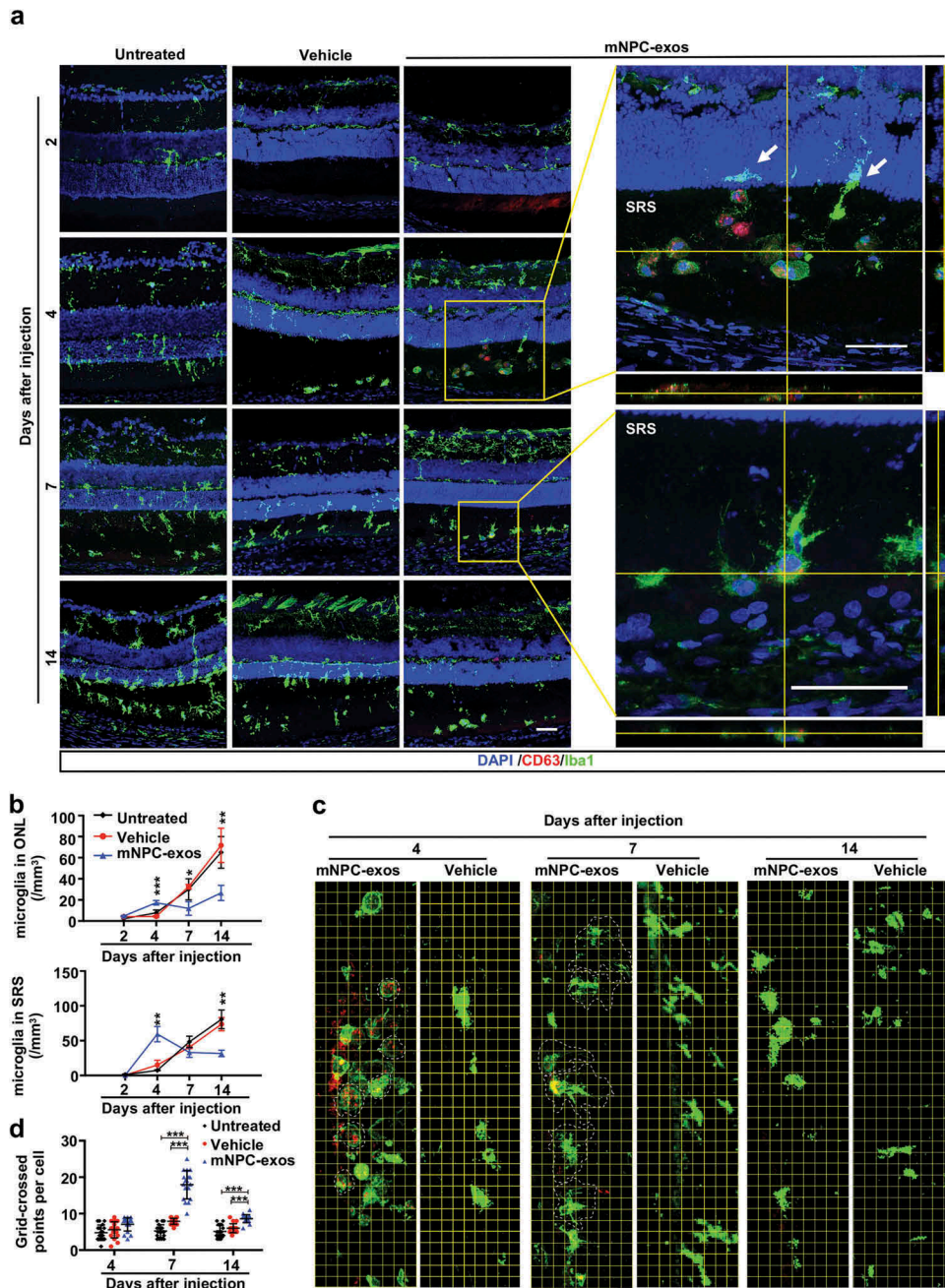


Figure 3. mNPC-exos suppressed the activation of microglia in the retina of RCS rats.

(a) Iba1 (green) staining in RCS retinas of untreated (left panel), treated with vehicle (middle panel) or CD63-RFP labelled mNPC-exos (right panel) at each time point. Enlarged orthogonal views of mNPC-exos (red) injected area at day 4 (upper-enlarged) and day 7 (lower-enlarged) show the mNPC-exos co-located with round (day 4) or ramified (day 7) microglia in subretinal space (SRS). See also Movie S2. (b) Statistical analysis of density of Iba1 positive microglia in ONL (upper panel) and SRS (lower panel) counted in confocal images ($n = 3$ eyes per group) of three groups. Data are shown as mean \pm SD. Untreated vs vehicle: no significant. mNPC-exo vs Vehicle: * $P < 0.05$, ** $P < 0.01$, *** $P < 0.001$. (c) Representative images and grid-cross analysis of Iba1 (green) positive microglia in SRS after injection of vehicle or mNPC-exos (red) and grid-cross analysis of microglia in SRS at 4, 7 and 14 days post injection. (d) Statistical analysis of the grid-crossing points per individual microglia in SRS after vehicle or mNPC-exos treatment at each time point ($n = 18$ per group). Data are shown as mean \pm SD. Untreated vs vehicle: no significant. mNPC-exo vs Vehicle: *** $P < 0.001$.

pathway, AMPK signalling, production of nitric oxide and reactive oxygen species in macrophages, NF- κ B signalling, PI3 K/AKT signalling, STAT3 pathway, IL-

6 signalling, IL-7 signalling pathway, TNFR2 signalling, role of IL-17 F in allergic inflammatory airway diseases, Toll-like receptor signalling, IL-17A

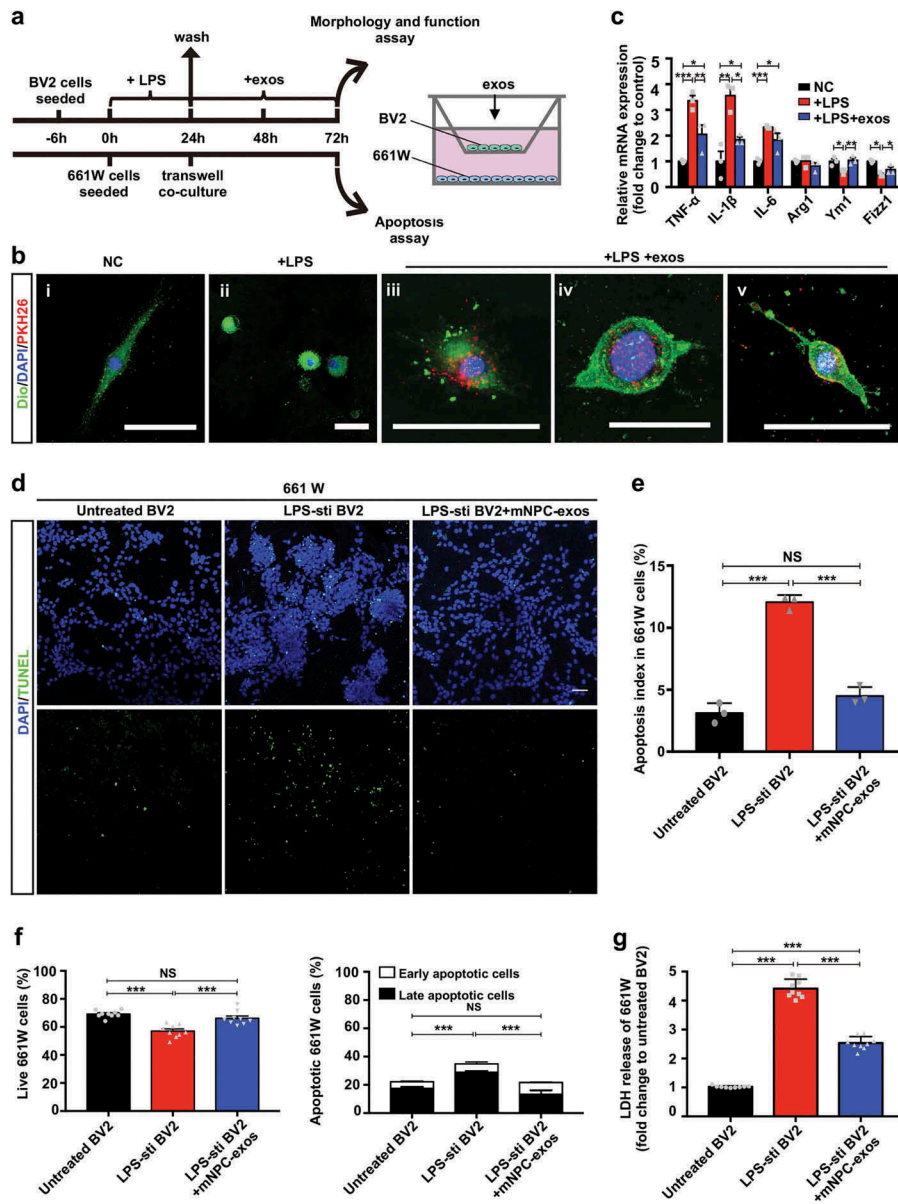


Figure 4. Inhibition of microglial activation by mNPC-exos protect photoreceptors *in vitro*.

(a) Scheme and diagram showing the co-culture system of BV2 cells and 661 W cells and the assays *in vitro*. (b) Representative confocal images show the morphology of Dio-labelled BV2 cells (green) cultured in the transwell chamber as negative control (i), stimulated with LPS (ii), and internalized of PKH26-labelled mNPC-exos (red) after LPS-stimulation (iii, iv, v). Scale bar, 50 μ m. (c) RT-qPCR analysis showing relative mRNA expression levels of TNF- α , IL-1 β , IL-6, Arg1, Ym1 and Fizz1 compared to the negative control (n = 3 per group). Data are shown as mean \pm SD. (d) Apoptosis detection with TUNEL (green) staining in 661 W cells. Nuclei were stained with DAPI. Scale bar, 500 μ m. (e) The apoptosis was increased in +BV2 LPS treated group compared with +BV2 untreated group, while mNPC-exos treatment reduced the apoptosis index in the +BV2 LPS treated +exos group (n = 3 per group). Data are shown as mean \pm SD. (f) Flow cytometry analysis with Annexin V and PI staining (supplement Fig 3) for percentage of live 661 W cells (left) and percentage of apoptotic 661 W cells (right). (n = 9 per group). (g) LDH release of 661 W of three groups. Data are normalized to +BV2 untreated group (n = 9 per group). Data are shown as mean \pm SD. *P < 0.05, **P < 0.01, ***P < 0.001. NC, negative control. LPS-sti, LPS-stimulated. NS, not significant.

signalling in airway cells, LPS-stimulated MAPK signalling, p38 MAPK signalling, JAK/Stat signalling (Figure 5(d)). Together, these results indicate that mNPC-exos inhibit several inflammation signal pathways in the LPS-activated microglia.

mNPC-exos contain miRNAs downregulating production of pro-inflammatory factors from activated microglia

To identify the molecular mechanisms by which mNPC-exos inhibit activation of microglia, we performed a sRNA-

sequencing and analysed the miRNA expression pattern. IPA with most abundant miRNAs in the first quartile range, downregulated mRNAs and focusing on the activation of microglia in BV2 cells showed that a set of 17 miRNAs (let-7a-5p, miR-26a-5p, miR-21-5p, miR-181a-5p, miR-30a-3p, miR-146a-5p, miR-328-3p, miR-24-3p, miR-103-3p, miR-17-5p, miR-125b-1-3p, miR-149-5p, miR-16-5p, miR-101-3p, miR-377-5p, miR-185-5p, miR-501-3p) could directly target three genes (TNF- α , IL-1 β and COX-2) that activated microglia (Figure 6(a, b)). RT-qPCR validated that LPS stimulation significantly elevated the mRNA levels of TNF- α , IL-1 β and COX-2, which were blocked by mNPC-exos in BV2 cells (Figure 6(c)). Corresponding changes in concentrations of TNF- α , IL-1 β and COX-2 in culture supernatant were observed (Figure 6(d)). These findings suggest that mNPC-exos enrich inflammation inhibitive miRNAs and may effectively suppress the activation of microglia.

hNPC-exos share the set of miRNAs with mNPC-exos to inhibit microglial activation

Previous studies have shown that the improvement of visual function in RD animal models and patients caused by grafted hNPCs could be partly attributed to immunomodulation [6,13]. Moreover, our experiments showed that hNPCs secreted exosomes after transplantation, suggesting hNPC-exos may be important mediators in hNPC therapy. To investigate whether hNPC-exos contained inflammatory inhibition-associated miRNAs similar to those in mNPC-exos, we isolated exosomes from hNPCs. These were positive for classical neural stem cell markers such as Nestin, PAX6 and SOX2 and negative for markers of differentiated retinal cells, including RECOVERIN, GS and GFAP at P4 (Figure S6). The isolated exosomes were positive for HSP70, CD9 and CD81 (Figure 7(a)) and showed a typical cup-shape with a double membrane (Figure 7(b)). We then performed sRNA-seq of hNPC-exos and analysed the miRNA expression pattern. Comparison of miRNA composition between hNPC-exos and mNPC-exos showed that 256 miRNAs (24.03%) were common for both hNPC-exos and mNPC-exos, and 285 (26.85%) and 523 miRNAs (49.10%) were unique for mNPC-exos and hNPC-exos, respectively (Figure 7(c), Table S3). Moreover, 11 of the top 20 abundant miRNAs were the same in hNPC-exos and mNPC-exos (Figure 7(d)). Interestingly, hNPC-exos contained the set of 17 miRNAs in mNPC-exos with 26.61% in hNPC-exos (Figure 7(e), Table S3) and 15.41% in mNPC-exos (Figure 6(b)), which were predicted to inhibit microglial activation through targeting TNF- α , IL-1 β and COX-2 (Figure 7(e), Table S3). Treated LPS-stimulated human

microglia cell hmgSV40 with hNPC-exos significantly blocked the expression of TNF- α , IL-1 β and COX-2 up-regulated by LPS stimulation (Figure 7(f)). These findings suggest that hNPC-exos contain the miRNAs similar to mNPC-exos and inhibit LPS-activated human microglia by targeting TNF- α , IL-1 β and COX-2.

Discussion

Transplantation of NPCs is a promising therapeutic strategy for neurodegenerative disorders, including RD, and transplantation of hNPCs is therapeutic in RD models. In the current study, we found that grafted hNPCs secreted CD63 positive EVs and exosomes in the SRS of an RD model. We also confirmed through OKT and scotopic ERG testing that direct administration of mNPC-exos preserved the visual function of RCS rats. Morphologically, mNPC-exos decreased the amount of apoptosis in photoreceptors and delayed the thinning of the ONL. We observed a transient reduction of b-wave amplitudes in mNPC-exo and vehicle groups at days 2 and 4, which was most likely due to the acute injury caused by the injection procedure [43], while the apoptosis of photoreceptors in mNPC-exo group reduced markedly compared to that of the vehicle and the untreated group. The mNPC-exo group had higher amplitudes of both a-wave and b-wave than that of the vehicle and the untreated groups at days 7 and 14, indicating the visual-protective effects of mNPC-exos, which was consistent with the anti-apoptosis results in Figure 1(h). It was reported that even the vehicle injection, as a sham surgical intervention, could provide a photoreceptor protective effect in a limited time [44–46]. And this might be the reason that the ONL of vehicle groups had less apoptosis cells compared to the untreated groups at days 7 and 14 post-injection in our study (Figure 1(h)). Moreover, the scotopic fERG (Figure 1(d, e)) is one of the frequently used measurements to record the light-driven electrical response from the entire retina [47], instead of reflecting the response of the localized and specific parts of the retina. So the maintenance of amplitudes of a-wave and b-wave didn't reflect exactly the partial anti-apoptosis effects, which might be the reason that the vehicle group partially had less apoptotic cells than the untreated group at days 7 and 14 post-injection, while the amplitudes of a-wave and b-wave of the entire retinas were similar. Our results provide, for the first time, evidence that the exosomes derived from NPCs could serve as a novel agent for RD treatment. Used for this purpose NPC-exos could be not only an effective therapy, but also potentially avoid the limitations of NPC transplantation, such as the lack of donors, risk of

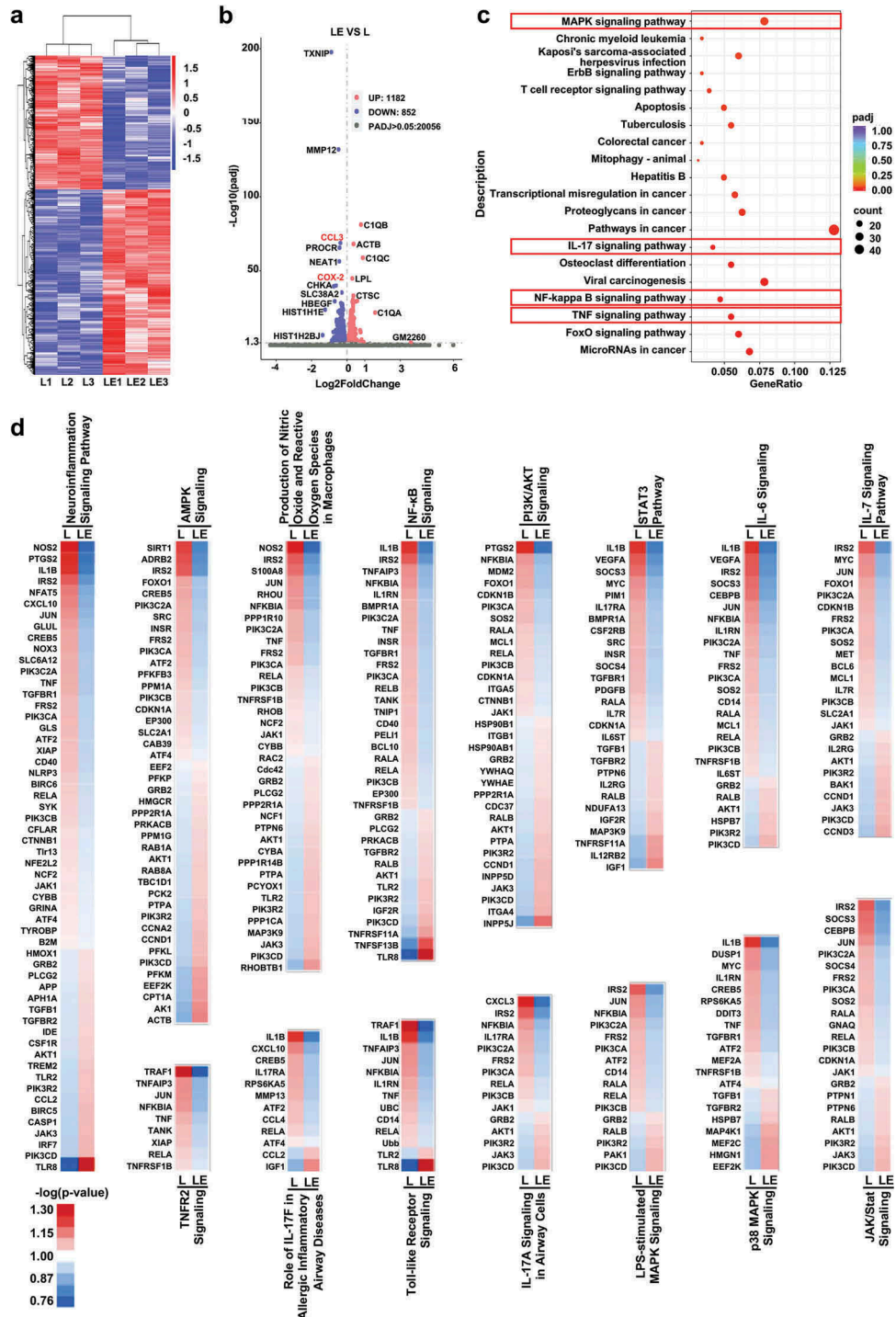


Figure 5. mNPC-exos inhibit inflammation signal pathway in the LPS-activated microglia.

(a) Heatmap of 2034 genes differentially expressed in LPS activated BV2 microglia cells treated with or without mNPC-exos. L: LPS-stimulated BV2 cells. LE: LPS-stimulated and mNPC-exo treated BV2 cells. (b) Volcano plot [x-axis = \log_2 (fold change); y-axis = $-\log_{10}$ (padj)] showing statistically significant differentially expressed genes compared to L group. The vertical dashed line ($x = 0$) separate the upregulated ($x > 0$) from the downregulated ($x < 0$) genes. The horizontal line ($y = 1.3$) correspond to a P -value = 0.05. Data have been calculated from $n = 3$ individual experiment per group. (c) The bubble chart shows enriched downregulated genes in KEGG signalling pathway. The Y-axis label represents the pathway and the X-axis label represents the rich factor (rich factor = amount of differentially expressed genes enriched in the pathway/amount of all genes in background gene set). The colour and size of the bubble represent enrichment significance and the amount of differentially expressed genes enriched in the pathway, respectively. (d) Ingenuity pathway analysis (IPA) of mNPC-exos regulated genes in LPS activated BV2 microglia cells. Heatmaps of selected immune and inflammation-related pathways of predicted inhibition rate (z -score < 0) are shown. Blue represents down-regulation of gene expression and red represents upregulation of gene expression.

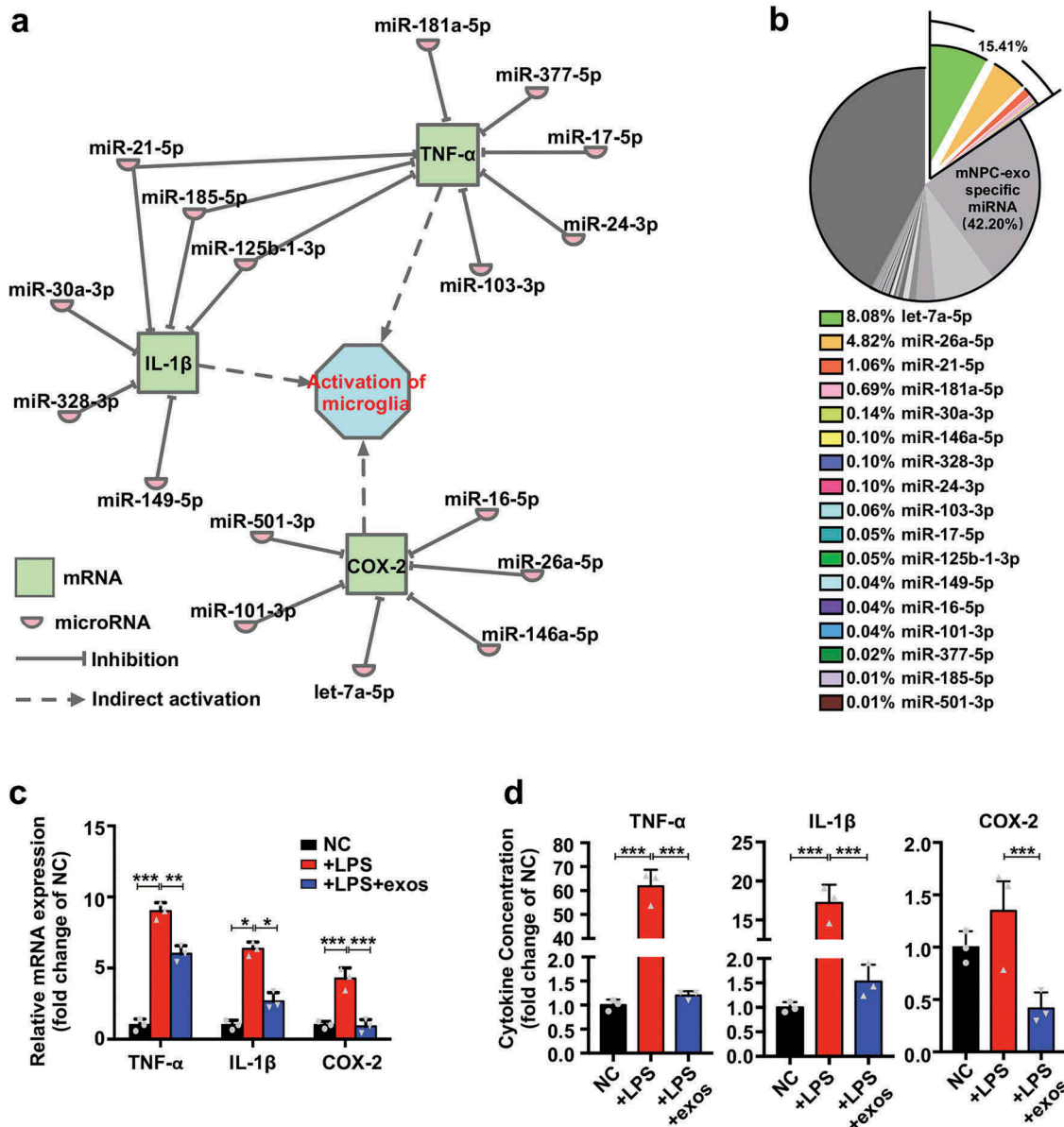


Figure 6. mNPC-exos contain miRNAs downregulating production of pro-inflammatory factors from activated microglia.

(a) Molecular network focused on activation of microglia from the correlation analysis between miRNAs in mNPC-exos and mRNAs in BV2 microglia cells identified through IPA. (b) Pie chart showing mNPC-exos contained miRNA abundance by small RNA sequencing. The 17 miRNAs targeting TNF- α , IL-1 β and COX-2 are colour-labelled and the corresponding proportions are listed below. (c) RT-qPCR analysis showing relative mRNA levels of TNF- α , IL-1 β and COX-2 in negative control (NC) group, +LPS group and +LPS+exos group ($n = 3$ per group). The level of mRNA expression was normalized to GAPDH and graphed relative to the NC group. Data are shown as mean \pm SD. (d) Concentrations of in BV2 microglia culture medium were measured by ELISA from the NC group, +LPS group and +LPS+exos group. Data were normalized to NC group. Data are shown as mean \pm SD ($n = 3$ per group). Data are shown as mean \pm SD. * $P < 0.05$, ** $P < 0.01$, *** $P < 0.001$.

teratoma formation, autoimmune responses, and religious or ethical concerns.

The most distinctive function of exosomes is intercellular communication within the microenvironment [48]. The mechanisms of this communication include signalling via membrane-to-membrane interaction with downstream cells [25] and signalling after endocytosis by target cells [49,50]. With labelled

mNPC-exos, we traced grafted exosomes and showed that they were internalized by microglia rather than Müller cells, RPE cells or photoreceptors in the ONL in RSC rats. This result is consistent with a report by Frühbeis et al. [51], in which exosomes derived from oligodendrocytes could be internalized by microglia, rather than by oligodendrocytes or astrocytes. Frühbeis et al. also observed that the exosomes

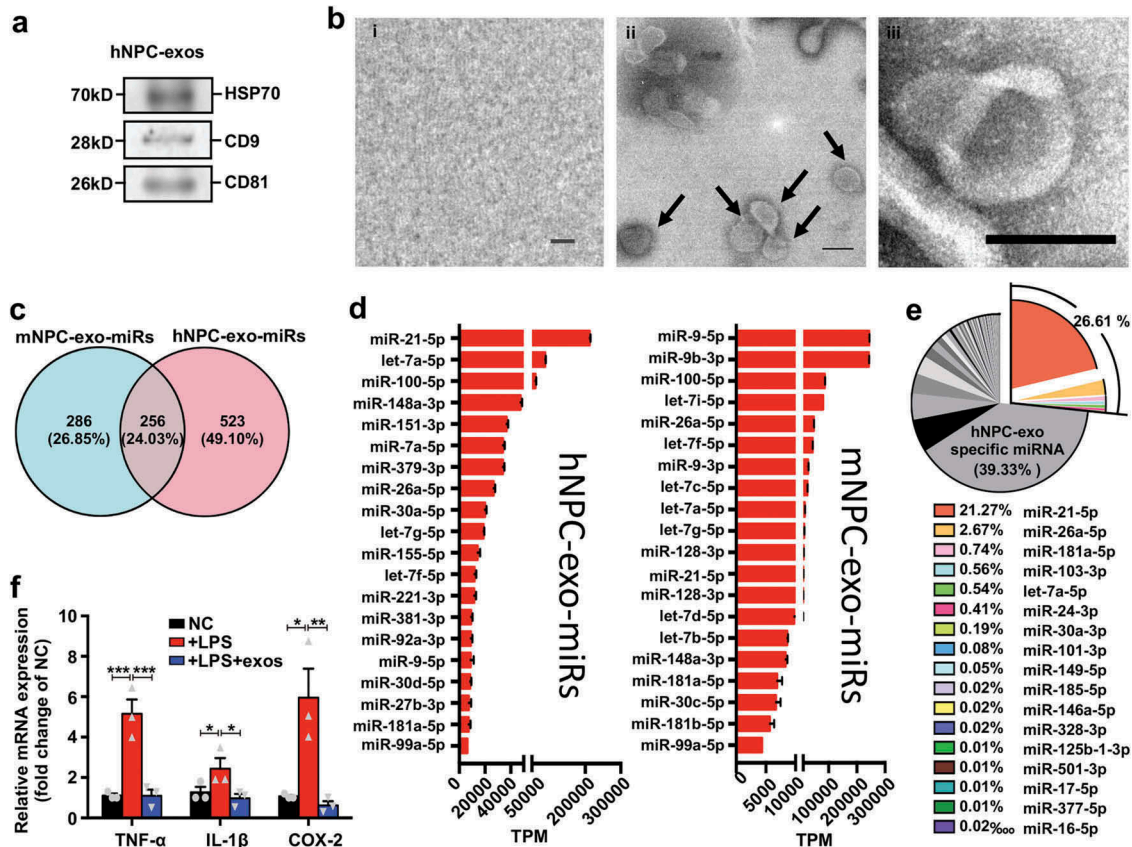


Figure 7. hNPC-exos contain miRNAs similar to mNPC-exos to inhibit microglial activation.

(a) Western blot results of HSP70, CD9, CD81 in hNPC-exos. (b) Transmission electron microscopy (TEM) of hNPC-exos (ii, iii, black arrowed) and control (i, PBS). Scale bars, 200 μ m. (c) Venn diagrams of the numerical values and percentage for the indicated common and different expressed miRNAs in hNPC-exos compared with mNPC exos. (d) miRNA abundance analysis by small RNA sequencing. Left panel shows the top 20 abundant miRNAs in hNPC-exos. Right panel shows the top 20 abundant miRNAs in mNPC-exos. (e) Pie chart showing hNPC-exos contained miRNA abundance by small RNA sequencing. The 17 miRNAs targeting TNF- α , IL-1 β and COX-2 are colour-labelled and the corresponding proportions are listed below. (f) RT-qPCR analysis showing relative mRNA levels of TNF- α , IL-1 β and COX-2 in negative control (NC) group, +LPS group and +LPS +exos group ($n = 3$ per group). The level of mRNA expression was normalized to GAPDH and graphed relative to the NC group. Data are shown as mean \pm SD.

could be internalized by cortical neurons but were preferentially internalized by microglia. As NPCs secrete several types of neurotrophic factors including nerve growth factor (NGF), brain-derived neurotrophic factor (BDNF), and ciliary neurotrophic factor (CNTF) within EVs specialized cargoes [52], and NPC-EVs can reach the degenerative or injured nervous tissue very quickly and directly transferred bioactive materials to the cells [53], we speculate that the neurotrophic factors released from the injected mNPC-exos also produce protection on the degenerative photoreceptor before the mNPC-exos are internalized by the microglia 4 days after injection. This might be part of the reason for the difference that the protection effect of mNPC-exo on photoreceptors occurred at day 2 post-injection, while the obvious accumulation and internalization were observed at day 4 post-injection.

Previous studies have reported that NPC-EVs were taken up by microglia and regulated microglial morphology and function during brain development [35]. It has also been reported that microglial activation and associated inflammatory responses impact the progression of RD [54,55]. However, it has not been clarified whether NPC-derived EVs or exosomes influence microglia in CNS disorders. In the present study, we found that grafted exosomes recruited microglia to the site of injection and activated microglia, which presented as a rounded shape that was consistent with that reported by Morton et al [35]. Interestingly, Morton et al. observed rounded microglia up to day 7, while we found that the rounded microglia returned to ramified shape at day 7 post-injection of mNPC-exos (48 hours incubation of exosomes *in vitro*), and the density of microglia in the ONL and SRS decreased in our model. This difference might be attributed to the

different models of physiological development and degenerative disorder.

It has been reported that suppression or depletion of microglial activation could be neuroprotective in neurodegenerative disorders, including RD [56]. In the present study, we found that administration of mNPC-exos reduced the density and recovered the morphology of microglia. Nevertheless, some studies have suggested that depletion of microglia may be detrimental in neurodegenerative diseases, since microglia could clear up damaged cells to promote the recovery and functionality of injured tissue. Our previous work also found that sustained elimination of microglia with PLX treatment aggravated RD [57]. By avoiding long-term and excessive inhibitory treatments, the present study showed that mNPC-exos may be an efficient microglial modulator that may be a better approach for treating these sensitive and highly responsive cells to produce a more efficient biotherapeutic method for treating RD.

The activated microglia may promote the progression of RD by direct and indirect effects. Zhao et al [32] reported that inhibition of activated microglia delayed the progression of RD by reducing the microglial phagocytosis of living photoreceptors. In the present study, we observed that mNPC-exos inhibited the activated microglia to reduce the production of inflammatory and neurotoxic factors, which delayed the progression of RD by protecting photoreceptors from apoptosis. And our results partially clarified the mechanisms by which grafted NPCs indirectly protect photoreceptors from apoptosis at the early stage. Upon inhibition of microglia by mNPC-exos, many inflammation-related pathways were inactivated, mainly the TNF- α , IL-1 β and COX-2 signalling pathways.

Exosomes transfer functional proteins, mRNAs and miRNAs to target cells to mediate intercellular communication [58,59]. Recent studies have indicated that miRNAs packaged in exosomes are more stable than in other components and can resist degradation after they are secreted from cells. In the present study, we found that miR-181, miR-26, miR-9 and the let-7 family were highly enriched (top 20 most abundant) in mNPC-exos, which is consistent with the findings of Morton et al [35]. Moreover, we found that there was a set of 17 miRNAs in mNPC-exos that were predicted to inhibit microglial activation through targeting TNF- α , IL-1 β , and COX-2. The composition of miRNAs of hNPC-exos was similar to that of mNPC-exos, including the set of 17 miRNAs. hNPC-exos or mNPC-exos treatment could inhibit the expression of TNF- α , IL-1 β and COX-2 in LPS-stimulated microglia. Thus, exosomes might be ideal inhibitors of microglia for RD

treatment, and engineered exosomes could be developed to package desired miRNAs to target specific cells [23].

Compared to the transplantation of stem cells for RD therapy, we found that exosomes caused milder retinal detachment. This might be due to their smaller size, which was more conducive to diffusion around the injected area. Up to now, the functional or morphological changes during the first three weeks after transplantation of stem cells in RD models have not been reported. This may be due to the fact that grafted stem cells may be accumulated in the SRS during the first three or even 12 weeks [5]. Our data suggests that transplantation of exosomes takes a short time to exert beneficial effects. However, the effects of NPC-exos were limited due to their short retention time in a single injection, compared with the long-term effects of stem cell transplantation. Accordingly, further studies are required to completely understand the effects of multiple injections of NPC-exos, or to develop more convenient and efficient methods for NPC-exo application based on modification.

In summary, we demonstrated that grafted NPC-exos efficiently suppress the activation of retinal microglia to mediate protection against apoptosis of photoreceptors by NPCs in an RD model. Both mNPC-exos and hNPC-exos contain a set of 17 miRNAs that mainly target TNF- α , IL-1 β and COX-2 related inflammatory pathways to inactivate microglia. Our findings suggest that NPC-exos may partially mediate the therapeutic effects of NPC transplantation and potentially a promising agent for RD treatment.

Acknowledgments

We thank Dr. Stefano Pluchino for gifting the plasmids. Many thanks to Prof. Youhong Cui, Prof. Xindong Liu, Prof. Yong Liu, Prof. Tian Xue, Prof. Bo Peng, Prof. Xia Zhang and Prof. Xiaotang Fan for their comments on the earlier drafts of this paper. Thanks also to Dr. Xi Chen, Dr. Yan Fu, Dr. Langyue Xue, Dr. Jing Xie, Dr. Ting Zou, Dr. Jiaman Dai, Dr. Wenyi Liu, Mr. Weiping Liu, Ms. Shuai Wang, Miss. Luodan A, Mr. Fei Ni for their kindly assistance in the early research.

Author contributions

B.B., C.Z., Z.Y. and H.X. contributed to conception and design. B.B., X.H., C.R., L.G., Y.Z., Q.L. and M. C. performed the experiments. B.B., C.W., Y.F. and J. H. performed collection and assembly of data, data analysis and interpretation, manuscript writing. B.B., L.G. and Y. G. performed data analysis and interpretation.

Disclosure of interest

The authors report no conflict of interest.

Funding

This study was supported by funding from the National Key R&D Program of China (2018YFA01017302), the National Natural Science Foundation of China (31571065), the Military Key Program (BWS13C015), the Foundation of Southwest Hospital (SWH2016ZDCX1001), the National Basic Research Program of China (2013CB967002) and Military Medical Science and Technology Innovation Plan of Southwest Hospital (SWH2017YBXM-04).

ORCID

Baishijiao Bian  <http://orcid.org/0000-0002-0729-1555>
 Xiangyu He  <http://orcid.org/0000-0001-8115-3727>
 Yu Gong  <http://orcid.org/0000-0003-2190-0369>
 Lingling Ge  <http://orcid.org/0000-0002-1797-3752>
 Yuxiao Zeng  <http://orcid.org/0000-0003-1471-9887>
 Qiyou Li  <http://orcid.org/0000-0002-9355-2319>
 Haiwei Xu  <http://orcid.org/0000-0002-8840-7918>
 Zheng Qin Yin  <http://orcid.org/0000-0002-4253-7485>

References

- [1] Ratnapriya R, Chew EY. Age-related macular degeneration-clinical review and genetics update. *Clin Genet.* 2013;84:160–166.
- [2] Ferrari S, Di Iorio E, Barbaro V, et al. Retinitis pigmentosa: genes and disease mechanisms. *Curr Genomics.* 2011;12:238–249.
- [3] Liu Y, Xu HW, Wang L, et al. Human embryonic stem cell-derived retinal pigment epithelium transplants as a potential treatment for wet age-related macular degeneration. *Cell Discov.* 2018;4:50.
- [4] Wang S, Girman S, Lu B, et al. Long-term vision rescue by human neural progenitors in a rat model of photoreceptor degeneration. *Invest Ophthalmol Vis Sci.* 2008;49:3201–3206.
- [5] Luo J, Baranov P, Patel S, et al. Human retinal progenitor cell transplantation preserves vision. *J Biol Chem.* 2014;289:6362–6371.
- [6] Liu Y, Chen SJ, Li SY, et al. Long-term safety of human retinal progenitor cell transplantation in retinitis pigmentosa patients. *Stem Cell Res Ther.* 2017;8:209.
- [7] Jayakody SA, Gonzalez-Cordero A, Ali RR, et al. Cellular strategies for retinal repair by photoreceptor replacement. *Prog Retin Eye Res.* 2015;46:31–66.
- [8] Pearson RA, Hippert C, Graca AB, et al. Photoreceptor replacement therapy: challenges presented by the diseased recipient retinal environment. *Vis Neurosci.* 2014;31:333–344.
- [9] MacLaren RE, Pearson RA, MacNeil A, et al. Retinal repair by transplantation of photoreceptor precursors. *Nature.* 2006;444:203–207.
- [10] Qu Z, Guan Y, Cui L, et al. Transplantation of rat embryonic stem cell-derived retinal progenitor cells preserves the retinal structure and function in rat retinal degeneration. *Stem Cell Res Ther.* 2015;6:219.
- [11] Pearson RA, Gonzalez-Cordero A, West EL, et al. Donor and host photoreceptors engage in material transfer following transplantation of post-mitotic photoreceptor precursors. *Nat Commun.* 2016;7:13029.
- [12] Santos-Ferreira T, Llonch S, Borsch O, et al. Retinal transplantation of photoreceptors results in donor-host cytoplasmic exchange. *Nat Commun.* 2016;7:13028.
- [13] Zou T, Gao L, Zeng Y, et al. Organoid-derived C-Kit (+)/SSEA4(-) human retinal progenitor cells promote a protective retinal microenvironment during transplantation in rodents. *Nat Commun.* 2019;10:1205.
- [14] Li Z, Zeng Y, Chen X, et al. Neural stem cells transplanted to the subretinal space of rd1 mice delay retinal degeneration by suppressing microglia activation. *Cytherapy.* 2016;18:771–784.
- [15] Kobayashi T, Vischer UM, Rosnoble C, et al. The tetraspanin CD63/lamp3 cycles between endocytic and secretory compartments in human endothelial cells. *Mol Biol Cell.* 2000;11:1829–1843.
- [16] Thery C, Witwer KW, Aikawa E, et al. Minimal information for studies of extracellular vesicles 2018 (MISEV2018): a position statement of the International Society for Extracellular Vesicles and update of the MISEV2014 guidelines. *J Extracell Vesicles.* 2018;7:1535750.
- [17] Schindowski K, Belarbi K, Buee L. Neurotrophic factors in Alzheimer's disease: role of axonal transport. *Genes Brain Behav.* 2008;7 Suppl 1:43–56.
- [18] Stevanato L, Thanabalasundaram L, Vysokov N, et al. Investigation of content, stoichiometry and transfer of miRNA from human neural stem cell line derived exosomes. *PLoS One.* 2016;11:e0146353.
- [19] Webb RL, Kaiser EE, Scoville SL, et al. Human neural stem cell extracellular vesicles improve tissue and functional recovery in the murine thromboembolic stroke model. *Transl Stroke Res.* 2018;9:530–539.
- [20] Jaimes Y, Naaldijk Y, Wenk K, et al. Mesenchymal stem cell-derived microvesicles modulate lipopolysaccharides-induced inflammatory responses to microglia cells. *Stem Cells.* 2017;35:812–823.
- [21] Nargesi AA, Lerman LO, Eirin A. Mesenchymal stem cell-derived extracellular vesicles for renal repair. *Curr Gene Ther.* 2017;17:29–42.
- [22] Jo YY, Lee H-J, Kook S-Y, et al. Isolation and characterization of postnatal stem cells from human dental tissues. *Tissue Eng.* 2007;13:767–773.
- [23] Valadi H, Ekström K, Bossios A, et al. Exosome-mediated transfer of mRNAs and microRNAs is a novel mechanism of genetic exchange between cells. *Nat Cell Biol.* 2007;9:654–659.
- [24] Zhang L, Zhang S, Yao J, et al. Microenvironment-induced PTEN loss by exosomal microRNA primes brain metastasis outgrowth. *Nature.* 2015;527:100–104.
- [25] Cossetti C, Iraci N, Mercer T, et al. Extracellular vesicles from neural stem cells transfer IFN- γ via Ifngr1 to activate Stat1 signaling in target cells. *Mol Cell.* 2014;56:193–204.
- [26] Tan E, Ding X-Q, Saadi A, et al. Expression of cone-photoreceptor-specific antigens in a cell line derived from retinal tumors in transgenic mice. *Invest Ophthalmol Vis Sci.* 2004; 45:764–768

- [27] Ma W, ZHU X, DING X, et al. Protective effects of SS31 on tBHP induced oxidative damage in 661W cells. *Mol Med Rep.* 2015;12:5026–5034.
- [28] Qu L, Gao L, Xu H, et al. Combined transplantation of human mesenchymal stem cells and human retinal progenitor cells into the subretinal space of RCS rats. *Sci Rep.* 2017;7:199.
- [29] Artavanis-Tsakonas K, Love JC, Ploegh HL, et al. Recruitment of CD63 to *Cryptococcus neoformans* phagosomes requires acidification. *Proc Natl Acad Sci U S A.* 2006;103:15945–15950.
- [30] Mostoslavsky G, Kotton DN, Fabian AJ, et al. Efficiency of transduction of highly purified murine hematopoietic stem cells by lentiviral and oncoretroviral vectors under conditions of minimal in vitro manipulation. *Mol Ther.* 2005;11:932–940.
- [31] Patel AB, Tsilioni I, Leeman SE, et al. Neurotensin stimulates sortilin and mTOR in human microglia inhibitable by methoxyluteolin, a potential therapeutic target for autism. *Proc Natl Acad Sci U S A.* 2016;113: E7049–E7058.
- [32] Zhao L, Zabel MK, Wang X, et al. Microglial phagocytosis of living photoreceptors contributes to inherited retinal degeneration. *EMBO Mol Med.* 2015;7:1179–1197.
- [33] Lückoff A, Scholz R, Sennlaub F, et al. Comprehensive analysis of mouse retinal mononuclear phagocytes. *Nat Protoc.* 2017;12:1136–1150.
- [34] Chen M, Zhao J, Luo C, et al. Para-inflammation-mediated retinal recruitment of bone marrow-derived myeloid cells following whole-body irradiation is CCL2 dependent. *Glia.* 2012;60:833–842.
- [35] Morton MC, Neckles VN, Seluzicki CM, et al. Neonatal subventricular zone neural stem cells release extracellular vesicles that act as a microglial morphogen. *Cell Rep.* 2018;23:78–89.
- [36] Cuenca N, Pinilla I, Sauve Y, et al. Early changes in synaptic connectivity following progressive photoreceptor degeneration in RCS rats. *Eur J Neurosci.* 2005;22:1057–1072.
- [37] Strauss O. The retinal pigment epithelium in visual function. *Physiol Rev.* 2005;85:845–881.
- [38] Zhou T, Huang Z, Zhu X, et al. Alpha-1 antitrypsin attenuates M1 microglia-mediated neuroinflammation in retinal degeneration. *Front Immunol.* 2018;9:1202.
- [39] Fumagalli M, Lombardi M, Gressens P, et al. How to reprogram microglia toward beneficial functions. *Glia.* 2018;66:2531–2549.
- [40] Byrnes KR, Stoica B, Loane DJ, et al. Metabotropic glutamate receptor 5 activation inhibits microglial associated inflammation and neurotoxicity. *Glia.* 2009;57:550–560.
- [41] Costa Verdera H, Gitz-Francois JJ, Schiffelers RM, et al. Cellular uptake of extracellular vesicles is mediated by clathrin-independent endocytosis and macropinocytosis. *J Control Release.* 2017;266:100–108.
- [42] Mulcahy LA, Pink RC, Carter DR. Routes and mechanisms of extracellular vesicle uptake. *J Extracell Vesicles.* 2014;3:1–14.
- [43] Tzameret A, Sher I, Belkin M, et al. Transplantation of human bone marrow mesenchymal stem cells as a thin subretinal layer ameliorates retinal degeneration in a rat model of retinal dystrophy. *Exp Eye Res.* 2014;118:135–144.
- [44] Silverman MS, Hughes SE. Photoreceptor rescue in the RCS rat without pigment epithelium transplantation. *Curr Eye Res.* 1990;9:183–191.
- [45] Sharma R, Bose D, Maminishkis A, et al. Retinal pigment epithelium replacement therapy for age-related macular degeneration: are we there yet? *Annu Rev Pharmacol Toxicol.* 2020;60:553–572.
- [46] McGill TJ, Cottam B, Lu B, et al. Transplantation of human central nervous system stem cells - neuroprotection in retinal degeneration. *Eur J Neurosci.* 2012;35:468–477.
- [47] Lamba DA, Gust J, TA R. Transplantation of human embryonic stem cell-derived photoreceptors restores some visual function in Crx-deficient mice. *Cell Stem Cell.* 2009;4:73–79.
- [48] Simons M, Raposo G. Exosomes-vesicular carriers for intercellular communication. *Curr Opin Cell Biol.* 2009;21:575–581.
- [49] Martino G, Pluchino S, Bonfanti L, et al. Brain regeneration in physiology and pathology: the immune signature driving therapeutic plasticity of neural stem cells. *Physiol Rev.* 2011;91:1281–1304.
- [50] Pluchino S, Cossetti C. How stem cells speak with host immune cells in inflammatory brain diseases. *Glia.* 2013;61:1379–1401.
- [51] Fruhbeis C, Fröhlich D, Kuo WP, et al. Neurotransmitter-triggered transfer of exosomes mediates oligodendrocyte-neuron communication. *PLoS Biol.* 2013;11:e1001604.
- [52] Willis CM, Nicaise AM, Peruzzotti-Jametti L, et al. The neural stem cell secretome and its role in brain repair. *Brain Res.* 2020;1729:146615.
- [53] Colombo M, Raposo G, Thery C. Biogenesis, secretion, and intercellular interactions of exosomes and other extracellular vesicles. *Annu Rev Cell Dev Biol.* 2014;30:255–289.
- [54] Yoshida N, Ikeda Y, Notomi S, et al. Clinical evidence of sustained chronic inflammatory reaction in retinitis pigmentosa. *Ophthalmology.* 2013;120:100–105.
- [55] Karlstetter M, Ebert S, Langmann T. Microglia in the healthy and degenerating retina: insights from novel mouse models. *Immunobiology.* 2010;215:685–691.
- [56] Peng B, Xiao J, Wang K, et al. Suppression of microglial activation is neuroprotective in a mouse model of human retinitis pigmentosa. *J Neurosci.* 2014;34:8139–8150.
- [57] He J, He J, Zhao C, et al. Microglia mediate synaptic material clearance at the early stage of rats with retinitis pigmentosa. *Front Immunol.* 2019;10:912.
- [58] Li J, Liu K, Liu Y, et al. Exosomes mediate the cell-to-cell transmission of IFN-alpha-induced antiviral activity. *Nat Immunol.* 2013;14:793–803.
- [59] Lv LL, Cao Y, Liu D, et al. Isolation and quantification of microRNAs from urinary exosomes/microvesicles for biomarker discovery. *Int J Biol Sci.* 2013;9:1021–1031.